Acta Pharmaceutica Sinica B 2022;12(2):890–906

Chinese Pharmaceutical Association
Institute of Materia Medica, Chinese Academy of Medical Sciences

Acta Pharmaceutica Sinica B

www.elsevier.com/locate/apsb
www.sciencedirect.com

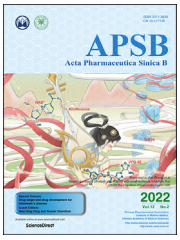

ORIGINAL ARTICLE

Antrodia cinnamomea exerts an anti-hepatoma effect by targeting PI3K/AKT-mediated cell cycle progression *in vitro* and *in vivo*

Yan Zhang[a,b,†], Pin Lv[c,†], Junmei Ma[b,†], Ning Chen[c], Huishan Guo[c], Yan Chen[d], Xiaoruo Gan[c], Rong Wang[c], Xuqiang Liu[d], Sufang Fan[b], Bin Cong[a,e,*], Wenyi Kang[d,*]

[a]*Hebei Key Laboratory of Forensic Medicine, College of Forensic Medicine, Hebei Medical University, Shijiazhuang 050017, China*
[b]*Hebei Food Safety Key Laboratory, Hebei Food Inspection and Research Institute, Shijiazhuang 050091, China*
[c]*Cardiovascular Medical Science Center, Department of Cell Biology, Hebei Medical University, Shijiazhuang 050017, China*
[d]*National R & D Center for Edible Fungus Processing Technology, Henan University, Kaifeng 475004, China*
[e]*Research Unit of Digestive Tract Microecosystem Pharmacology and Toxicology, Chinese Academy of Medical Sciences, Beijing 100730, China*

Received 6 May 2021; received in revised form 5 July 2021; accepted 9 July 2021

KEYWORDS

Antrodia cinnamomea;
UPLC–Q-TOF/MS;
Anti-hepatocellular carcinoma;
Network pharmacology;
PI3K/AKT;
Cell cycle

Abstract *Antrodia cinnamomea* is extensively used as a traditional medicine to prevention and treatment of liver cancer. However, its comprehensive chemical fingerprint is uncertain, and the mechanisms, especially the potential therapeutic target for anti-hepatocellular carcinoma (HCC) are still unclear. Using UPLC–Q-TOF/MS, 139 chemical components were identified in *A. cinnamomea* dropping pills (ACDPs). Based on these chemical components, network pharmacology demonstrated that the targets of active components were significantly enriched in the pathways in cancer, which were closely related with cell proliferation regulation. Next, HCC data was downloaded from Gene Expression Omnibus database (GEO). The Cancer Genome Atlas (TCGA) and DisGeNET were analyzed by bioinformatics, and 79 biomarkers were obtained. Furtherly, nine targets of ACDP active components were revealed, and they were significantly enriched in PI3K/AKT and cell cycle signaling pathways. The affinity between these targets and their corresponding active ingredients was predicted by molecular docking. Finally, *in vivo* and *in vitro* experiments showed that ACDPs could reduce the activity of PI3K/AKT signaling pathway

*Corresponding authors. Tel./fax: +86 311 86266406; +86 371 23880680.
E-mail addresses: hbydcongbin@126.com (Bin Cong), kangweny@hotmail.com (Wenyi Kang).
[†]These authors made equal contributions to this work.
Peer review under responsibility of Chinese Pharmaceutical Association and Institute of Materia Medica, Chinese Academy of Medical Sciences.

https://doi.org/10.1016/j.apsb.2021.07.010

and downregulate the expression of cell cycle-related proteins, contributing to the decreased growth of liver cancer. Altogether, PI3K/AKT-cell cycle appears as the significant central node in anti-liver cancer of *A. Cinnamomea*.

1. Introduction

Hepatocellular carcinoma (HCC) has been known as the most frequent subtype of liver cancer, and is the fourth cause of cancer-related mortality worldwide[1,2], not only due to the high rate of spread, metastases and recurrence, but also to the dismal treatment effect. At present, a variety of drugs, such as sorafenib and regorafenib, improve the overall survival rate of HCC patients. However, these drugs have some problems, including short time effect, drug resistance, and other problems. Therefore, it is urgent to find new drugs with safety, high efficiency, low toxicity and reversing drug resistance.

As a mainstream form of complementary and alternative medicine, traditional Chinese medicine (TCM) has been widely accepted for cancer patients because of its beneficial effects and lack of serious side effects[3]. *Antrodia cinnamomea* is a rare fungus that grows in Taiwan, China, distributing over broad-leaved forests at an altitude of 200−2000 m. Pharmacological studies have shown that *A. cinnamomea* has anti-tumor, liver protection, immune regulation, inhibiting vascular neointimal formation, lowering blood pressure and cholesterol, inhibiting platelet aggregation, and other physiological activities[4−9]. Of the numerous functions, the effects of hepatoprotective especially anti-HCC were the most often reported. *A. cinnamomea* could reduce HCC cell viability, proliferation, migration and invasion, and induce apoptosis[10−14]. However, the predominant role and the mechanism of *A. cinnamomea* in anti-HCC have not been elucidated.

Nowadays, *A. cinnamomea* is commercially available in the form of fermented wine or pure cultures in powdered, tablet, dropping pill and capsule form, and has gradually become one of the most popular hepatoprotective agents and health products in Taiwan[15−17]. Recent studies showed that *A. cinnamomea* contains a variety of physiologically active compounds, including terpenoids, adenosine, organic germanium, trace elements, proteins, ergosterol, vitamins, nicotinic acid, nucleic acid lectins, chitin, lignin, etc.[7,8,18]. However, current reports about the chemical fingerprint of *A. cinnamomea* are scattered, and the systematic study is lacking. Furthermore, the studies on *A. cinnamomea* are mostly focused on the therapeutic effects or quantitative analysis of individual components[19−24]. From a holistic perspective, the comprehensive chemical fingerprint and the correlations among the chemical composition, molecular targets, signaling pathway and anti-HCC activity have remained elusive.

In the current work, using UPLC−Q-TOF/MS, we identified, for the first time, that there are 139 chemical components in *A. cinnamomea* dropping pills (ACDPs), including 102 terpenoids, eight benzenoids, two purine nucleosides and 27 other classes. Next, according to network pharmacology, we showed that CCNB1, CASP8, CCNE1, CDK1, PIK3CA, MET, AURKA, TOP2A and TERT might be the potential protein targets, and KEGG pathway enrichment analysis revealed that they were significantly enriched in PI3K/AKT and cell cycle signaling pathway. Lastly, *in vivo* and *in vitro* experiments verified that ACDPs inhibited the proliferation of HCC in the dose- and time-dependent manner, the activity of PI3K/AKT signaling pathway was decreased, accompanied with the downregulated expression of cell cycle-related proteins.

2. Materials and methods

2.1. Preparation of ACDPs methanol extract and UPLC–Q-TOF/MS analysis

ACDPs were supplied by Greathealer Healthcare Technology Company Limited (Taiwan, China). The ACDPs samples were crushed into powder through a 50 mesh screen. One grams ACDPs sample was weighted and placed in 50 mL centrifuge tube, and then the sample was extracted with 20 mL methanol (Darmstadt, Germany). After vortexing for 1 min and sonicating for 30 min, the mixture was centrifuged at 10,000 r/min for 5 min. 1 mL supernatant was filtered using a 0.22 μm nylon membrane before UPLC–Q-TOF/MS analysis. UPLC analysis was completed with LC-30AD UPLC system (Shimadzu Corporation, Kyoto, Japan), while mass spectrometry was implemented by a hybrid quadrupole time-of-flight tandem mass spectrometer Q-TOF/MS (Triple TOF™ 5600$^+$ MS system, AB Sciex Corporation., Foster City, CA, USA).

2.2. Strategy of identification and characterization of compounds

Sciex OS software (version 1.5.0, Sciex, USA) was employed to analyze the results of UPLC–Q-TOF/MS. Utilizing Triple TOF™5600$^+$ MS system, the mass accuracy of all acquired ions were less than 5 ppm, and their exact isotopic pattern could be determined. Therefore, the molecular formula was determined easily by accurate mass and isotopic abundance ratio, using "formula finder function" of Sciex OS 1.5.0 software. The fragmentation behavior of the compound with similar structure was investigated, and then the rules were applied to the structural elucidation of their derivatives with the same basic structure. The compound structure was determined mainly through calculating the exact mass of MS/MS fragments and comparing those fragments with compounds from the TCM MS/MS database and on-line Chemspider database using Sciex OS 1.5.0 software or literature. The TCM MS/MS database with 1320 components was supplied by AB Sciex Corporation., and the on-line Chemspider database can perform on-line analysis of more than 44 million compounds, and will be constantly updated.

2.3. *Target prediction of ACDPs active ingredients*

As shown on of Fig. 1, the active ingredients of ACDPs were screened by the SwissADME programme (http://swissadme.ch/index.php)[25]. First, gastrointestinal absorption (GI absorption) was set as "HIGH" as the condition for drug absorption, which was used to screen active compounds with good oral bioavailability. Secondly, two or more compounds with "YES" in the five predicted properties (Lipinski, Ghose, Veber, Egan, Muegge) can be regarded as active ingredients. According to the selected active ingredients, Swiss Target Prediction (http://swisstargetprediction.ch/) was applied to predict the possible targets[26]. Swiss TargetPrediction selected the targets whose probability is > 0.12 in the prediction results for further analysis. At the same time, experimentally verified targets information was downloaded from NPASS (http://bidd2.nus.edu.sg/npass/) and the entries related to the active components of ACDPs were extracted. Finally, target information was integrated and accumulated to obtain the possible targets of ACDPs active ingredients.

2.4. *Prediction for targets of HCC*

Download the gene expression profile data of HCC from Gene Expression Omnibus (GEO, https://portal.gdc.cancer.gov/) database, and the matrix meeting the following conditions would be used to screen the differential expression genes (DEGs): (1) the total sample size was greater than 80; (2) the tumor tissue and normal tissue samples were both included. GSE14520, GSE45267, GSE64041, and GSE112790 met the above conditions and were downloaded locally. FactoMineR, limma and pheatmap package in R software (version 4.0) were used in turn for principal component analysis (PCA), DEGs screening and cluster analysis. The DEGs (FDR$<$0.05 and $|\log_2 FC|>1$) were integrated with the RobustRankAgggreg (RRA) package and visualized by ggplot2. Liver Hepatocellular Carcinoma (LIHC) of The Cancer Genome Atlas (TCGA, https://portal.gdc.cancer.gov/) was used for testing the DEGs after integration. Survival analysis and Receiver Operating Characteristic (ROC) were completed by the survival and survivalROC package in the R software respectively. Genes that met the following conditions were targets for LIHC: (1) $P < 0.05$; (2) AUC$>$0.7. Download the proven HCC targets from DisGeNET (http://www.disgenet.org/home/) and merge them with predicted targets. Part of the technical route was shown in Fig. 1.

2.5. *Enrichment analysis of the common targets of ACDPs and HCC*

Take the intersection of the targets of ACDPs and HCC that play an anti-HCC role in ACDPs. These targets were imported into STRING (https://string-db.org) to construct protein−protein interaction network. The module analysis of the network was carried out by using the MCODE plug-in of Cytoscape (version

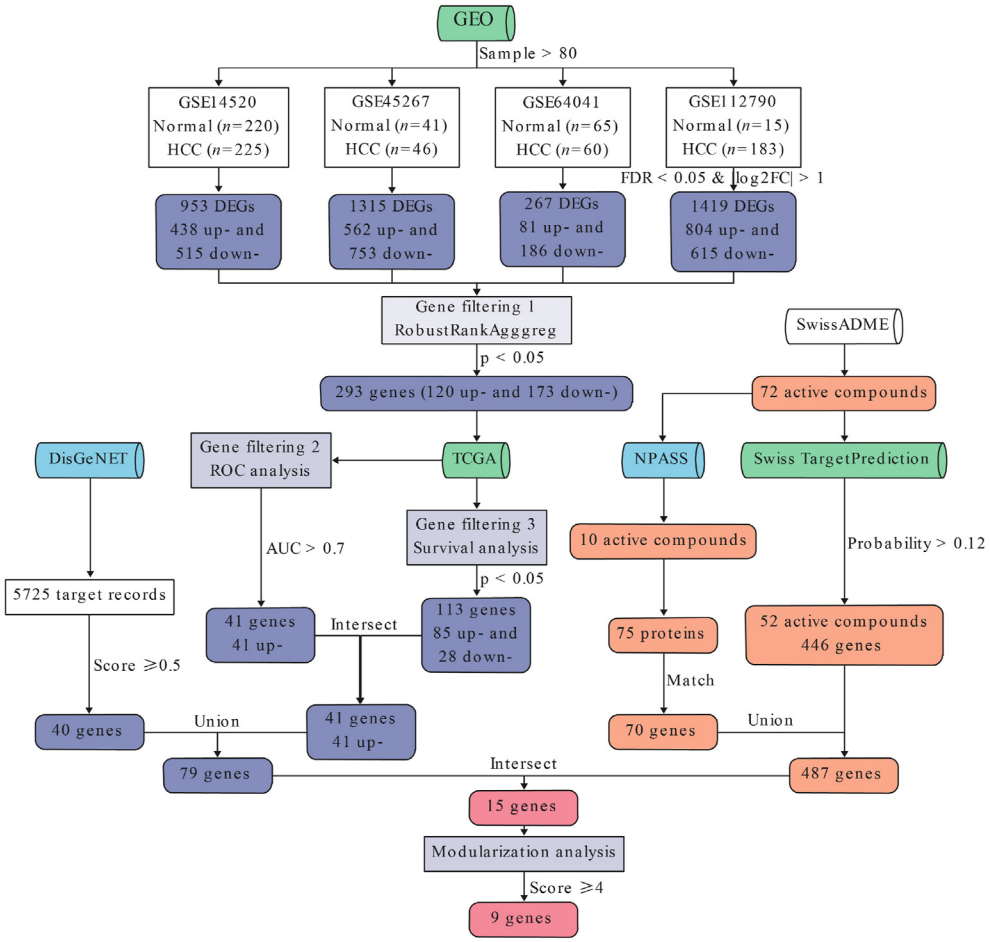

Figure 1 Flow chart of the prediction for targets of active components from ACDPs by bioinformatics.

3.7.1) and the DAVID (https://david.ncifcrf.gov/tools.jsp) was applied to GO and KEGG enrichment analysis.

2.6. Molecular docking studies

The molecular docking study was accomplished in Sybyl-X 2.0, and crystal structure of AURKA (PDB: 5ZAN), CASP8 (PDB: 4JJ7), CCNB1 (PDB: 2JGZ), CCNE1 (PDB: 6GU2), MET (PDB: 1CMB), CDK1 (PDB: 4YC3), PIK3CA (PDB: 6PYS), TERT (PDB: 1X2B) and TOP2A (PDB: 5NNE) was obtained from the RCSB Protein Data Bank. All polar hydrogen atoms were added and solvation parameters were assigned. Before the docking process, the ligand substructures were extracted and water molecules were removed. The surflex-dock total score was expressed in $-\log K_d$ to represent binding affinities. The higher docking total score, the stronger interaction of proteins and bioactive compounds.

2.7. Cell culture and treatment

The human hepatoma cell lines HepG2, Huh-7 and SMMC-7721 were purchased from Cell Bank of the Chinese Academy of Science (Shanghai, China). HepG2 cells were cultured in MEM media, Huh-7 cells and SMMC-7721 cells were cultured in RPMI1640. All of the medium supplement with 10% FBS (*v*/*v*) and 1% penicillin-streptomycin in a humid atmosphere with 5% CO_2 at 37 °C.

2.8. Cell viability assay

CCK-8 assay was carried out to determine cell viability as previously described[27]. Cells were seeded onto 96-well plates (5×10^3 cells per well) with each experiment being repeated 6 times. After being incubated at 37 °C for 24 h, cells were treated with various concentrations of ACDPs for 24 or 48 h. Next, 10 μL CCK-8 reagent was added into each well for another 1 h of incubation at 37 °C following the manufacturer's instructions (Beyotime, China). Then, optical density (OD) values were measured at 450 nm using a microplate reader.

2.9. EdU assay

EdU assay was carried out to determine cell proliferation as previously described[28]. Cells were cultured on coverslips, and then treated by 3.2 mg/mL ACDPs for 24 h. Next, EdU was added onto each coverslip and incubated for 2 h. After that, cells were incubated with stationary liquid (PBS containing 4% polyoxymethylene) at room temperature for 30 min, followed by incubation with glycine for 5 min and permeabilized with penetrating agent (PBS containing 0.5% TritonX-100) for 10 min. After being washed with PBS, the cells were treated with Apollo staining reaction liquid (RiboBio, China) for 30 min followed by the addition of penetrating agent and methanol for washing. Cells were subsequently washed with PBS and added with Hoechst 33,342 reaction reagents for 30 min. Apollo and 4′,6-dimidyl-2-phenylindole were screened to record EdU-positive cells by confocal microscope.

2.10. Colony formation experiment

The steps of colony formation experiment were as follows: 3000 cells/well were seeded and treated with different concentrations of ACDPs. After 1 weeks of culture with medium, the colonies were clearly visible. On top of that, colonies were fixed with 4% polyoxymethylene, stained with crystal violet, photographed and counted with Image J software.

2.11. Western blot analysis

Cells were prepared with lysis buffer (1% Triton X-100, 150 mmol/L NaCl, 10 mmol/L Tris-HCl, pH 7.4, 1 mmol/L EDTA, 1 mmol/L EGTA, pH 8.0, 0.2 mmol/L Na_3VO_4, 0.2 mmol/L phenylmethylsulfonyl fluoride (PMSF), and 0.5% nonidet P (NP)-40). Equal amounts of protein (60−100 μg) were separated by 10% SDS-PAGE and electro-transferred on to a polyvinylidenefluoride (PVDF) membrane. Membranes were blocked with 5% non-fat milk in tris-buffered saline-Tween (TBST) for 2 h at room temperature and incubated with specific primary antibodies against cyclin E1 (1:500, sc-377,100, Santa Cruz), CDK1 (1: 500, ab265590, Abcam), PIK3CA (1:500, sc-293,172, Santa Cruz), AKT1 (1:500, sc-5298, Santa Cruz), p-AKT (1:500, #4060, Cell Signaling Technology), cleaved-caspase 8 (1:500, #8592P, Cell Signaling Technology), or tubulin (1:1000, ab7291, Abcam) at 4 °C overnight. The membranes were then incubated with HRP-conjugated secondary antibody (1:1000, Seracare) for 1 h at room temperature, following the blots were visualized using GE ImageQuant™ LAS 4000 detection system. The protein bands of interest were quantified using Quantity One software (Bio-Rad).

2.12. Animal and tumor allograft model

Eight-week-old BALB/c mice underwent a tumor-burdened experiment. For the experiment, mice were maintained in specific pathogen-free (SPF) environment with standard rodent chow, water and light−dark cycles every 12 h at constant room temperature. All animal procedures conformed to the Guide for the Care and Use of Laboratory Animals published by the National Institutes of Health, and were approved by the Institutional Animal Care and Use Committee of Hebei Medical University (Shijiazhuang, China).

The mice were randomly divided into three group: model group (normal saline NS: 0.1 mL/10 g/day); ACDPs high-dose group (400 mg/kg/day); ACDPs low-dose group (200 mg/kg/day). We injected 1×10^7 Huh-7 cells with phosphate buffer saline (PBS) subcutaneously into the skin above the right shoulder of mice. The mice were treated through intragastric administration for 9 days. And the body weights of mice and volumes of the tumors were measured every 3 days. Finally, the mice were sacrificed with cervical dislocation and tumors were collected for further analysis.

2.13. Haematoxylin and eosin (H&E) staining and immunohistochemistry

Tumor tissues were fixed with 4% polyoxymethylene, dehydrated by ethanol and placed in xylene, then embedded in paraffin wax and sliced. The sections were baked at 65 °C for 4 h, dewaxed, hematoxylin stained for 15 min, decolorized with hydrochloric acid alcohol solution for 5 s. And then we stained them with eosin for 2 min and made it dehydrated. Finally, we mounted them in neutral gel and observed the tumor tissue sections with microscope.

The immunohistochemical analyses were processed according to standard procedures. In short, the slices were baked and then

dewaxed in xylene and hydrated in gradient alcohol. Then, 3% H_2O_2 was added to the sections to remove endogenous peroxidase. Immunostained sections were preincubated with 5% normal goat serum and then incubated with specific primary antibodies against cyclin E1 (1:500, sc-377,100, Santa Cruz), CDK1 (1: 500, ab265590, Abcam), PIK3CA (1:500, sc-293,172, Santa Cruz), AKT1 (1:500, sc-5298, Santa Cruz), p-AKT (1:500, #4060, Cell Signaling Technology), cleaved-caspase 8 (1:500, #8592, Cell Signaling Technology). The sections were incubated with the horseradish peroxidase streptavidin biotinylated secondary antibody (Dako) followed by diaminobenzidine (DAB kit, Vector Laboratories). For the negative controls, the primary antibody was replaced with non-immune rabbit or mouse serum. Staining intensities were determined by measurement of the integrated optical density (IOD) with light microscopy using a computer-based Image-Pro Morphometric System. The results are expressed as the mean value of at least three randomly chosen slides in each group.

2.14. *Statistical analysis*

Data analysis was performed using SPSS version 16.0 or Graphpad Prism six software. Data are presented as means ± standard deviation (SD) from at least three independent experiments, and each independent experiment was repeated at least three times to obtain the mean. Normally distributed datasets were analyzed with the unpaired Student's *t*-test for two independent groups or paired *t* test for two dependent groups, and the one-way analysis of variance (ANOVA) followed by the post Bonferroni's multiple comparisons test for ≥3 groups. For all statistical comparisons, a value of $P < 0.05$ was considered statistically significant, and denoted with one, two and three asterisks when lower than 0.05, 0.01 and 0.001, respectively.

3. Results

3.1. *Identification and characterization of constituents of ACDPs*

The MS spectra were obtained in both positive and negative ion modes. The representative total ion chromatograms (TIC) are displayed in Supporting Information Fig. S1A and B. In positive mode, 17,764 spectra were obtained, and in negative mode, 11,496 spectra were obtained (Fig. S1C and D). Imported the data into Sciex OS 1.5.0 software, selected the ion with mass error less than 5 ppm, the isotope distribution was correct, and contain secondary fragments as the target ion for qualitative analysis. The compounds were rapidly selected by targeted and non-targeted peak finding approaches, and then tentatively identified by comparing with TCM MS/MS database, on-line Chemspider database or inferred through mass spectrometry fragment ion analysis and literature data. A total of 139 compounds were rapidly selected by targeted and non-targeted peak finding approaches, including 102 terpenoids, eight benzenoids, two purine nucleosides and 27 other classes. 139 chemical components listed in Supporting Information Table S1.

3.1.1. *Identification of terpenoids*

Many terpenoid compounds have been isolated from ACs recently and have significant anti-tumor activities and research values because their toxicity is much lower than that other compounds[29,30]. Predominant in ACDPs are generally terpenoids in a large number, including diterpenoids, triterpenoids, tetraterpenoids and keratosterol. Among them, triterpenoids are the main components. A common feature of these structures is ergostane or lanostane skeleton. In order to better understand the MS fragmentation pattern of terpenoids from ACDP constituents, we took compound **1** as an example, which showed $[M+H]^+$ ion at *m/z* 455.3152 on the TOF-MS spectrum. The molecular formula was speculated to be C29H42O4 based on the analysis of its elemental composition and fractional isotope abundance. The main fragment ions were analyzed *via* the TOF-MS/MS screening and the main fragment ions were analyzed *via* the MS/MS screening and observed at *m/z* 437 $[M + H{-}H_2O]^+$, 409 $[M + H{-}H_2O{-}CO]^+$, 297 $[M + H{-}H_2O{-}CO{-}C_8H_{16}]^+$, 205 $[M + H{-}H_2O{-}CO{-}C_{15}H_{24}]^+$ in the positive ion spectrum. These fragments were coincided with the reference substance antcin A. These fragments were coincided with the antcin A in the TCM MS/MS database. As such, compound **1** was finally identified to be antcin A. The mass spectra, fragment information and Sciex OS screening interface of antcin A in positive mode were illustrated in Fig. 2A and B.

For the components not in the TCM MS/MS database, analysis was conducted using the on-line Chemspider database, fragmentation pathway and literature data. We took compound **7** as an example, which showed a protonated ion $[M+H]^+$ at *m/z* 489.3207 with the molecular formula $C_{29}H_{44}O_6$ in the positive ionization mode. The hydrogen adduct $[M+H]^+$ was observed in positive ionization mode. Further MS/MS scan showed that they produced fragment ions at *m/z* 471.3101, 453.2986, 435.2878, 407.2930, 175.1478, etc. Compound **7** was identified as antcin K by comparing with on-line Chemspider database, inferred through mass spectrometry fragment ion analysis. The mass spectra and fragment information were illustrated in Fig. 2C.

102 terpenoid components listed in Table S1 were identified or inferred in ACDP. It can be seen that terpene alcohols are prone to continuous loss of H_2O and CO_2, and the research and analysis of the chemical structure showed that there was ring split phenomenon. Some compounds should be assigned as the isomers *via* their high-resolution mass values. For example, compounds **2** and **5** were preliminarily identified as antcin B, antcin F or zhankuic acid A by comparing with TCM MS/MS database and literature data. We checked with Chemspider and found that zhankuic acid A is the same as antcin B, consistent with the previous results[31]. Compounds **2** and **5** displayed a similar deprotonated ion $[M+H]^+$ at *m/z* 469.2944 and 469.2945 with the same molecular formula $C_{29}H_{40}O_5$. The fragment information of the two compounds was relatively similar. The *c*log*P* values of the antcin B and antcin F were calculated using ChemDraw software. Antcin F has smaller *c*log*P* value while antcin B has higher value. They were 4.687 and 5.362, respectively. The *c*log*P* value of one compound, which was the logarithm of its partition coefficient between *n*-octanol and water $\log(C_{octanol}/C_{water})$, was a well-established measure of a compound hydrophilicity. Therefore, antcin F was firstly eluted. Compound **5** was identified as antcin F, compound **2** was identified as antcin B (zhankuic acid A).

3.1.2. *Identification of benzenoids*

A total of eight benzenoids were identified. We took compound 108 as an example. Based on the analysis of its elemental composition and fractional isotope abundance, its molecular formula was predicted to be $C_{10}H_{12}O_4$. The precise molecular weight was 197.0808, and the main fragment ions were analyzed *via* the MS/MS screening and observed at *m/z* 167 $[M + H{-}CH_2O]^+$, 139

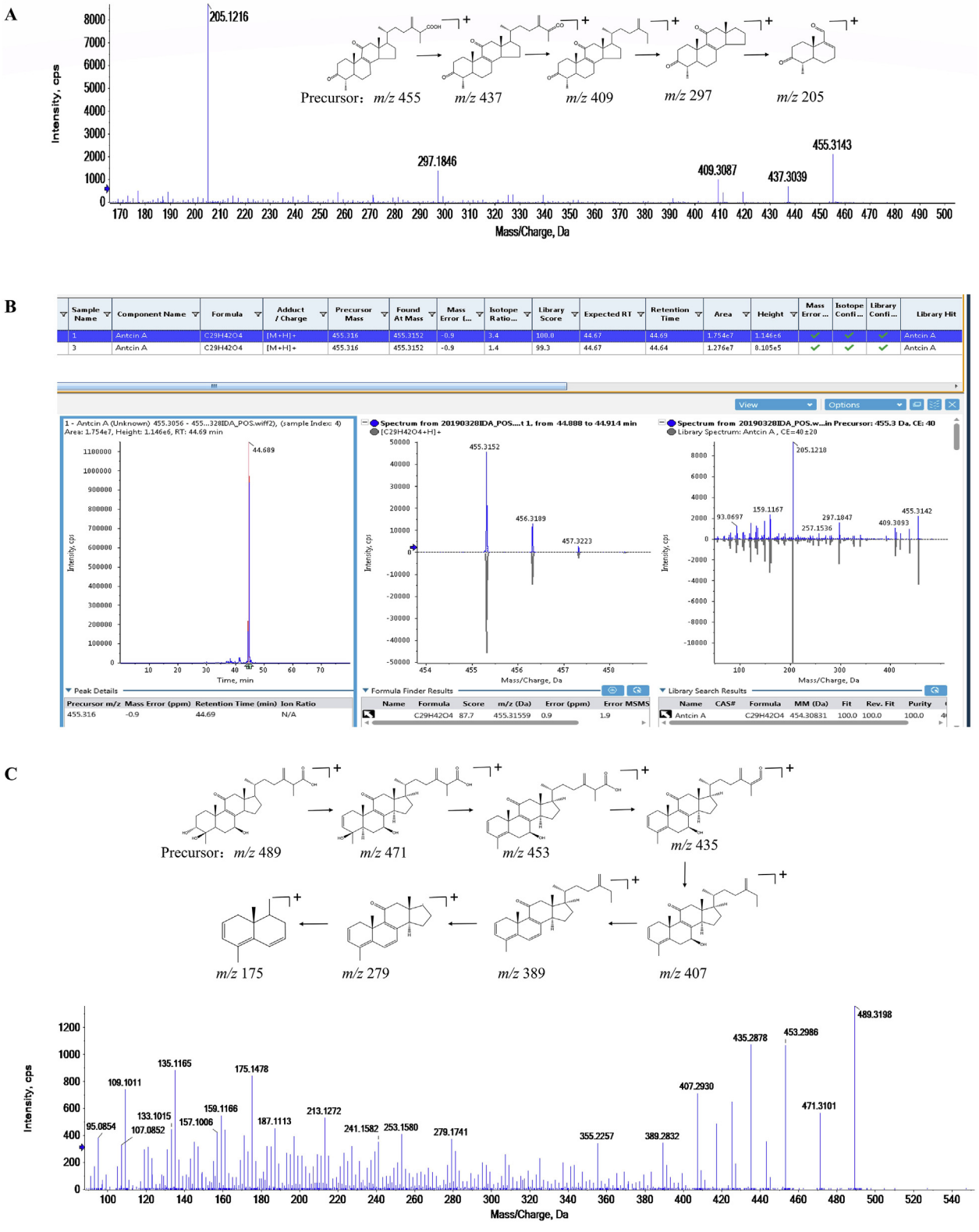

Figure 2 Identification result of chemical composition. (A) Mass spectra and fragmentation pathways of antcin A. (B) Sciex OS identification interface of antcin A. (C) Mass spectra and fragmentation pathways of antcin K.

$[M + H-C_2H_2O_2]^+$, 124 $[M + H-C_3H_5O_2]^+$, 109 $[M + H-C_4H_8O_2]^+$ and 77 $[M + H-C_4H_8O_4]^+$ in the positive ion spectrum. It was identified as 4,7-dimethoxy-5-methyl-1,3-benzodioxole by searching the database, inferred through mass spectrometry fragment ion analysis and literature data[23]. The mass spectra, fragmentation pathway and Sciex OS screening interface of 4,7-dimethoxy-5-methyl-1,3-benzodioxole in positive mode are illustrated in Supporting Information Fig. S2A and B.

3.1.3. Identification of nucleosides

As nitrogen-containing compounds, nucleoside compounds easily produce $[M+H]^+$ quasi-molecular ion peaks in positive ion mode. In secondary mass spectrometry, nucleosides are prone to lose ribose ($C_5H_8O_4$, 132 Da) or deoxyribose ($C_5H_8O_3$, 116 Da) to produce base quasi-molecular ion peaks. Compound **111** with the $[M+H]^+$ ion at *m/z* 268.1042, which produced the fragment ions at *m/z* 136 and *m/z* 119. The main fragment ions at *m/z* 136 was obtained by the loss of $C_5H_8O_4$ from the precursor ion at *m/z* 268, while the ion at *m/z* 119 was produced by continuous loss of NH_3. Based on the analysis of its elemental composition and fractional isotope abundance, its molecular formula was predicted to be $C_{10}H_{13}N_5O_4$. By searching the database, inferred through mass spectrometry fragment ion analysis and literature data, compound **111** was identified as adenosine. The mirror image matching diagram of secondary fragments of compound **111** and reference substance in TCM MS/MS database was illustrated in Fig. S2C and D.

3.1.4. Identification of other classes

In addition, 27 other compounds have been identified from ACDPs, including unsaturated fatty acids and vitamins, etc. Compound **139** was selected as an example. The precise molecular weight was 181.0722, and the main fragment ions were analyzed *via* the MS/MS screening and observed at *m/z* 163 $[M-H-H_2O]^-$, 101 $[M-H-C_2H_8O_3]^-$, 59 $[M-H-C_4H_{10}O_4]^-$, 89 $[M-H-C_3H_8O_3]^-$, and 71 $[M-H-C_3H_{10}O_4]^-$ in the negative ion spectrum. Based on the analysis of its elemental composition and fractional isotope abundance, its molecular formula was predicted to be $C_6H_{14}O_6$. According to the fragment information and TCM MS/MS database, the compound was identified as mannitol. The secondary fragment of this substance was consistent with the secondary fragment of the reference substance in the TCM MS/MS database. The mass spectra, fragment information and Sciex OS screening interface of mannitol in negative mode are illustrated in Supporting Information Fig. S3A and B.

For both aliphatic and aromatic carboxylic acids, their typical pattern of mass spectrometry is continuous loss of H_2O (18 Da) and CO_2 (44 Da). Took compound **115** as an example, the precise molecular weight was 133.0146, and the molecular formula was speculated to be $C_4H_6O_5$ based on the analysis of its elemental composition and fractional isotope abundance. Ion of 115 $[M-H-H_2O]^-$ fragment was generated by losing H_2O from $[M-H]^-$ ion. Then, 71 $[M-H-H_2O-CO_2]^-$ ion was formed through losing CO_2 from 115 $[M-H-H_2O]^-$ ion. Compound **115** was identified as malic acid by comparing with on-line Chemspider database, inferred through mass spectrometry fragment ion analysis and literature data[32]. The mass spectra and fragment information were illustrated in Fig. S3C.

3.2. Results of prediction and enrichment analysis of the active components of ACDPs

Firstly, the compounds in ACDPs were searched in the Swiss ADME database. There were 72 active ingredients with high gastrointestinal absorption and appropriate drug-likeness. Swiss TargetPrediction was used to predict the targets of compounds, and to construct the composition-target network (Fig. 3A and Supporting Information Table S2). At the same time, the information about the verified targets of ACDPs was downloaded, and the repeated targets were merged (Supporting Information Table S3). Then, the enrichment analysis of GO and KEGG after integration of all targets were shown in Fig. 3B and C and Supporting Information Table S4. GO enrichment analysis showed that the targets of ACDPs were closely related to positive regulation of ERK1 and ERK2 cascade, inflammatory response, negative regulation of apoptotic process, positive regulation of cell proliferation, and so on (Fig. 3B). KEGG pathway enrichment analysis indicated that the targets of ACDPs were significantly enriched in pathways in cancer, hepatitis B, FoxO signaling pathway, insulin resistance, and so on (Fig. 3C).

3.3. The results of prediction for biomarkers of HCC

514 HCC samples and 341 normal samples were acquired in the datasets of GSE14520, GSE45267, GSE64041, and GSE112790 (Supporting Information Table S5). As shown in Fig. 4A–D, the results of PCA suggested that tumor and normal tissue samples in each dataset came from different populations, which indicated that the source of the sample was reliable. Then, the results of different analysis of limma package (Supporting Information Table S6) were shown in Fig. 4E–H after visualization of ggplot2, and the heat map of differential expression genes (DEGs) were shown in Fig. 4I–L. The clustering results of heat map proved that the DEGs could distinguish tumor tissues and normal tissues, so the DEGs were representative of the whole sample. DEGs were integrated by RobustRankAggreg (RRA), and 293 DEGs, including 120 up- and 173 down-regulated genes, were obtained (Fig. 4M and Supporting Information Table S7). DKK1, REG3A, DEFB1, MMP12 and LCN2 were the top five up-regulated genes, while STAB2, CLEC1B, CXCL14, FCN3 and ASPM were the top five down-regulated genes.

The TCGA database contained 374 HCC tissues and 50 normal tissues. Survival analysis showed that 113 DEGs from patients with HCC were significantly related to overall survival (Supporting Information Table S8). ROC analysis showed that 41 DEGs from patients with HCC were significantly related to the identification of tumors (Supporting Information Table S9). In LIHC, the DEGs with significant influence on overall survival were AURKA, CCNB1, cyclin dependent kinase 1 (CDK1), SUMO-activating enzyme subunit 1 (SAE1) and topoisomerase IIα (TOP2A), and the corresponding ROC curves of these genes were shown in Fig. 5. By combining results from LIHC that were significant for overall survival and tumor identification, 41 DEGs (41 up-regulated genes) closely related to HCC were gained. Validated targets were downloaded from DisGeNET database and there were 5725 entries related to HCC. 40 HCC targets (Supporting Information Table S10) were gathered by setting the

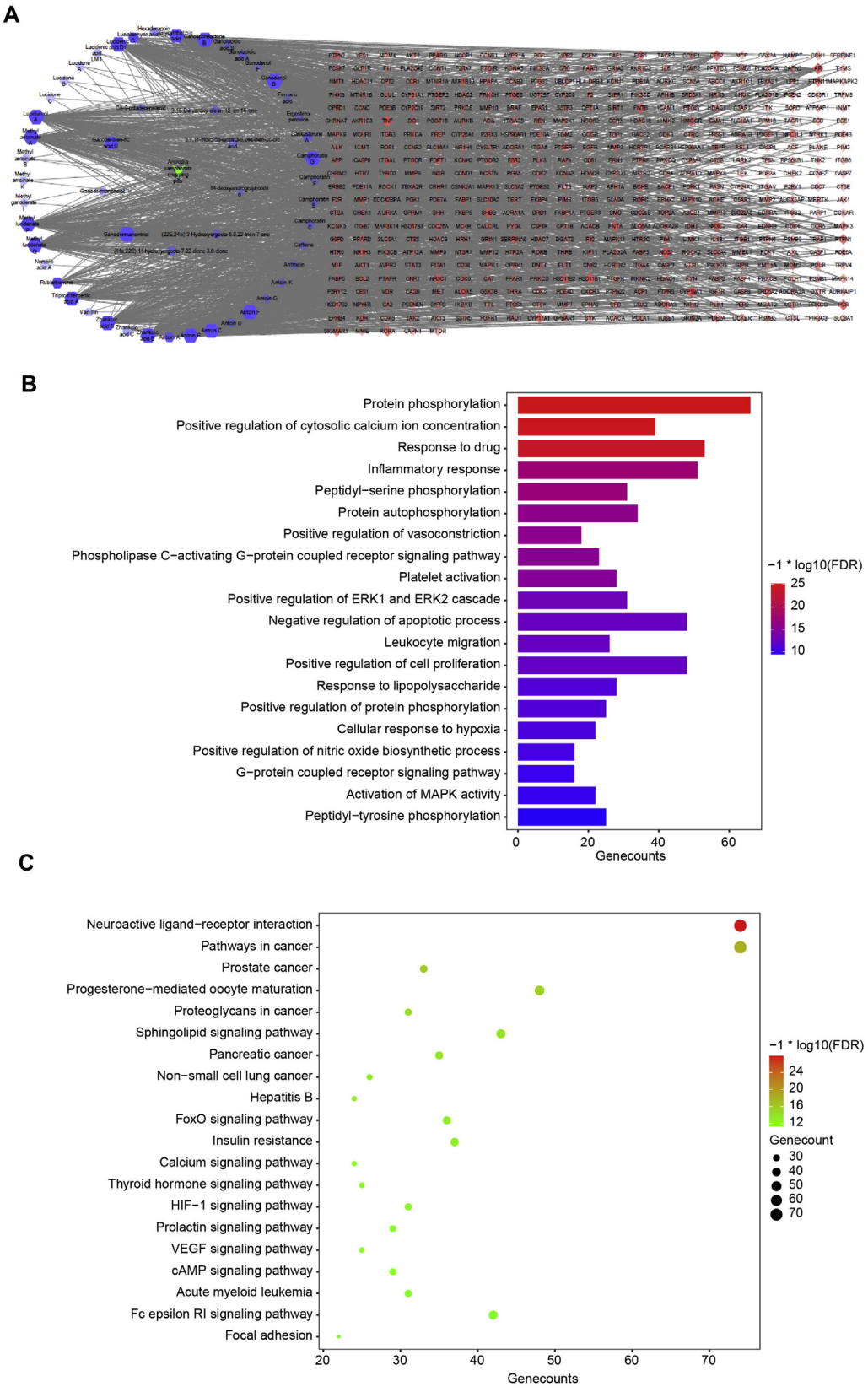

Figure 3 Results of targets of active components from ACDPs. (A) Component-target network diagram of ACDPs. (B) Histogram of GO enrichment analysis of targets. (C) Bubble chart of KEGG enrichment analysis of targets.

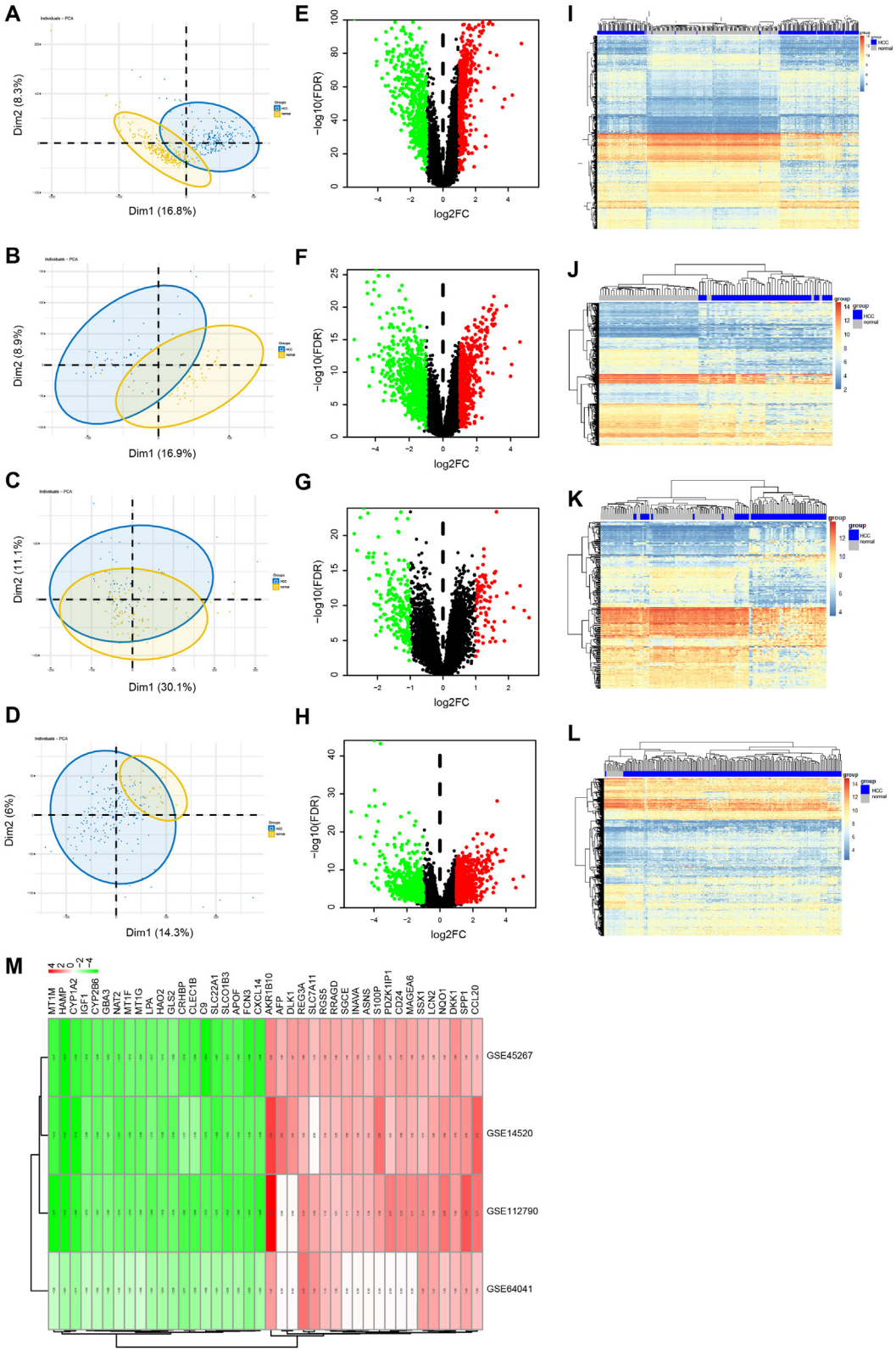

Figure 4 Results of DEGs in HCC related datasets in GEO database. (A)–(D) PCA diagram of GSE14520, GSE45267, GSE64041, and GSE112790. (E)–(H) Volcano map of DEGs in GSE14520, GSE45267, GSE64041, and GSE112790. (I)–(L) Heat map of DEGs in GSE14520, GSE45267, GSE64041, and GSE112790. (M) Heat map of TOP 20 up-regulated and down-regulated DEGs.

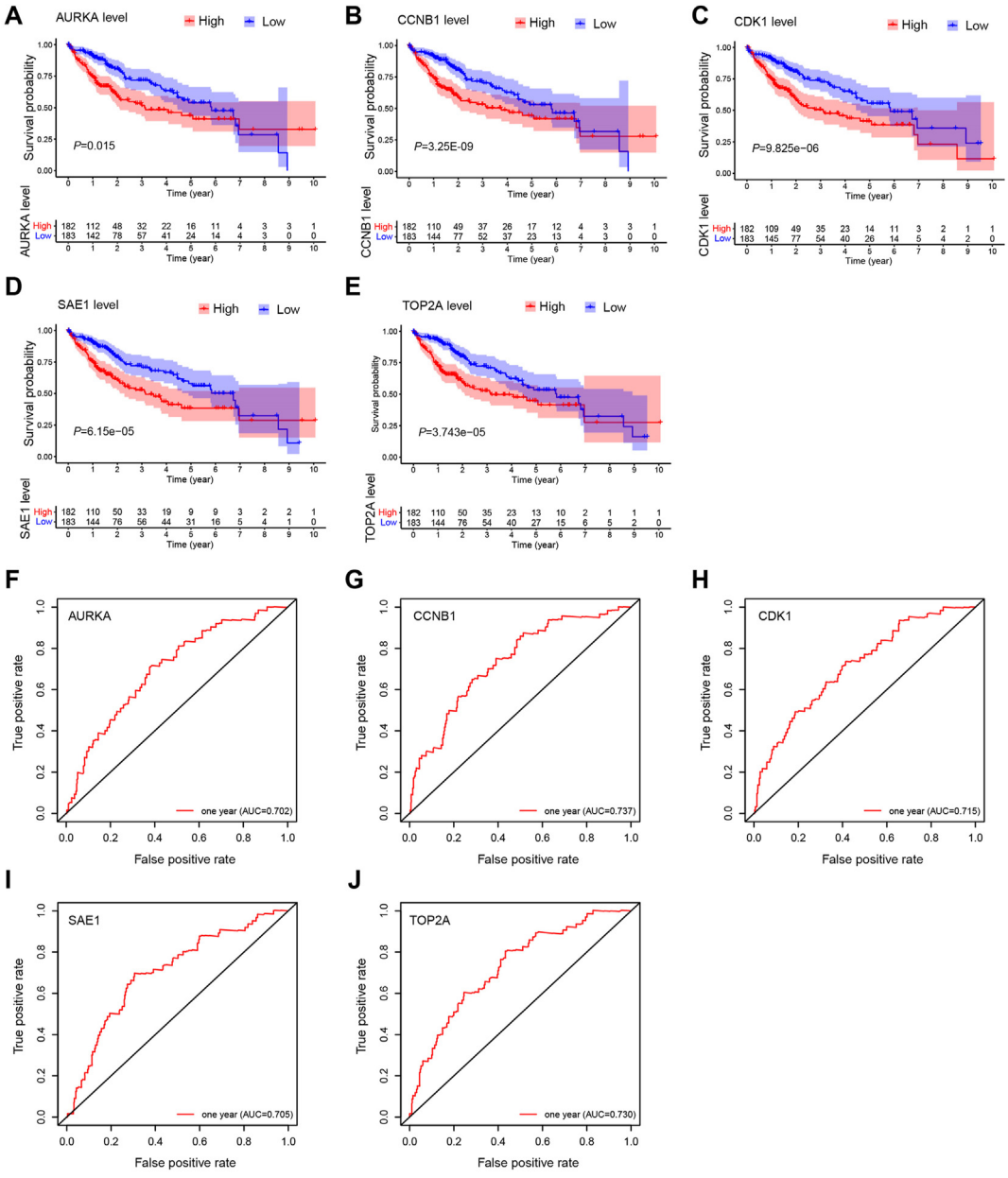

Figure 5 Results of DEGs filtered and selected by TCGA database. (A)–(E) Survival curves of AURKA, CCNB1, CDK1, SAE1 and TOP2A in HCC patients. (F)–(J) ROC curves of AURKA, CCNB1, CDK1, SAE1 and TOP2A in HCC patients.

threshold value to 0.5. Finally, 79 Biomarkers of HCC were obtained by merging these targets.

3.4. Results of enrichment analysis of the HCC-related targets of ACDPs

15 targets related to HCC in ACDPs were acquired from the intersection of ACDPs targets and HCC targets (Fig. 6A). Then we built the protein−protein interaction (PPI) network with STRING database and Cytoscape. Based on this, we used the MCODE plug-in to calculate the modules with special functions in the PPI network. nine targets, including CCNB1, CASP8, CCNE1, CDK1, PIK3CA, MET, AURKA, TOP2A and TERT, were gathered by modularization analysis score≥4. KEGG pathway enrichment analysis of these targets showed that they were significantly enriched in phosphoinositide-3 kinase (PI3K)/AKT and cell cycle signaling pathway, such as pathways in cancer, viral carcinogenesis, and P53 signaling pathway (Fig. 6B and Supporting Information Table S11). Meanwhile, the network of these targets with the active ingredients of ACDPs was shown in Fig. 6C. Then, a molecular docking approach was used to predict the interaction between ACDP bioactive compounds and corresponding target proteins. As shown in Supporting Information Table S12, zhankuic acid E had the potentially high binding affinity with CDK1, PIK3CA and CCNE1, ganoderiol B had the potentially high binding affinity with CDK1 and PIK3CA, ganodermanontriol had the potentially high binding affinity with CCNE1, lucidumol A had the potentially high binding affinity with TERT, and so on. Three- and two-dimensional binding mode of the active compounds and proteins were shown in Fig. 6D and E and Supporting Information Fig. S4. Taken together, these results indicated that ACDPs might play an anti-hepatoma role through decreasing the

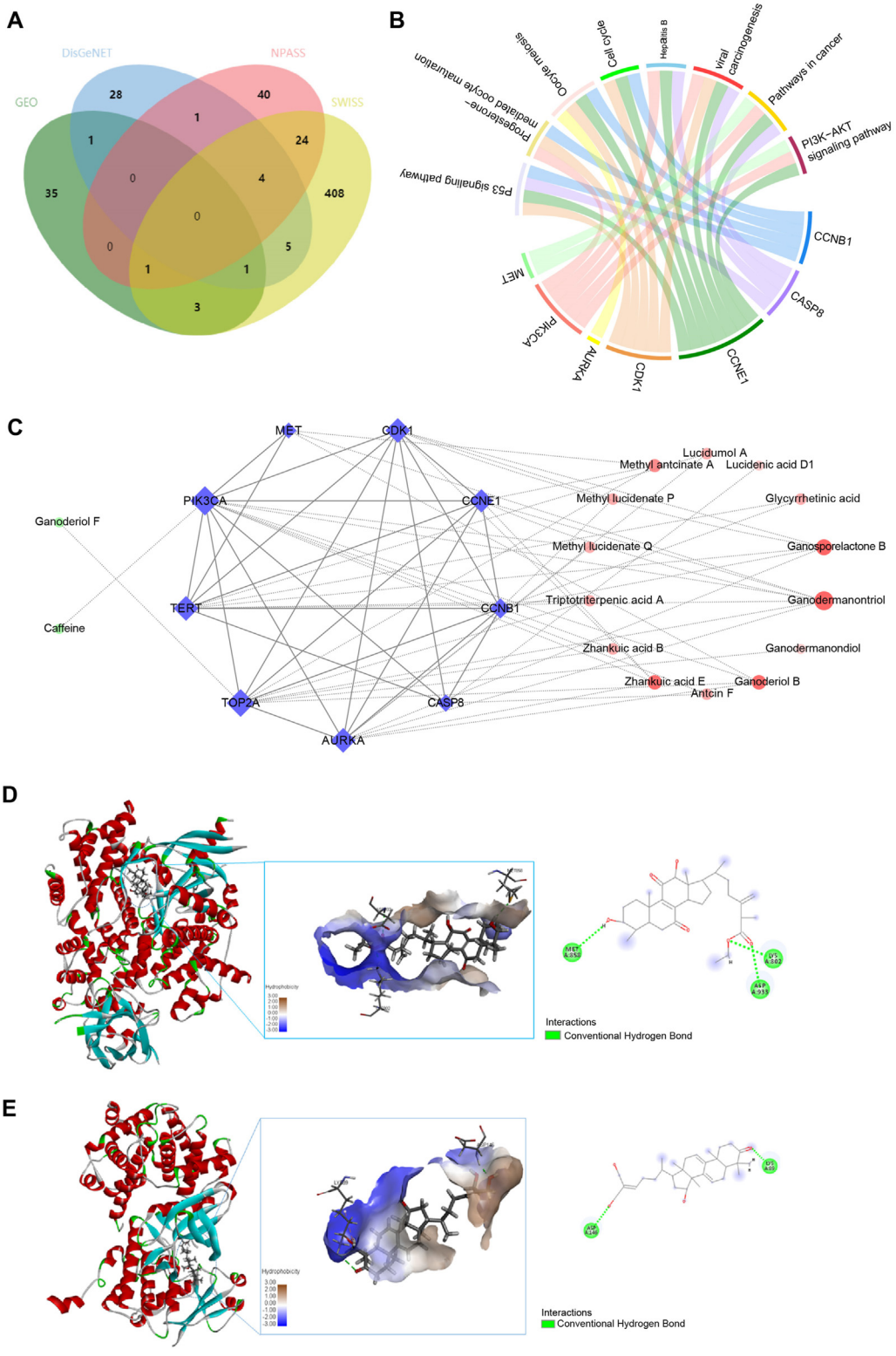

Figure 6 Results of enrichment analysis of the HCC-related targets of ACDPs. (A) Veen map of active ingredients and HCC targets. (B) Circos diagram of KEGG pathway enrichment analysis of the nine common targets. (C) Network of the nine common targets and ACDPs active ingredients. (D) Three-dimensional binding mode and two-dimensional binding mode of zhankuic acid E and PIK3CA (PDB: 6PYS). (E) Three- and two-dimensional binding mode of ganoderiol B and CDK1 (PDB: 4YC3).

expression of cell cycle-related protein regulated by the PI3K/AKT signaling cascade.

3.5. *ACDPs repress the proliferation of HCC cells in vitro through PI3K/AKT/cell cycle axis*

To further verify the effect of ACDPs on HCC cells, we turned to culture HepG2, Huh-7 and SMMC-7721, the human hepatoma cell lines. Firstly, we examined the effect of ACDPs on cell viability using the CCK-8 assay. Cells were pretreated with different concentrations (0, 0.4, 0.8, 1.6, and 3.2 mg/mL) of ACDPs for 24 or 48 h. As shown in Fig. 7A–C, treatment of cells with ACDPs dose- and time-dependently inhibited the viability of HCC cells. Then, the colony formation experiment further proved that ACDPs had reasonable anti-liver cancer effect *in vitro* (Fig. 7D), similar to the results of CCK-8 assays. Furtherly, the

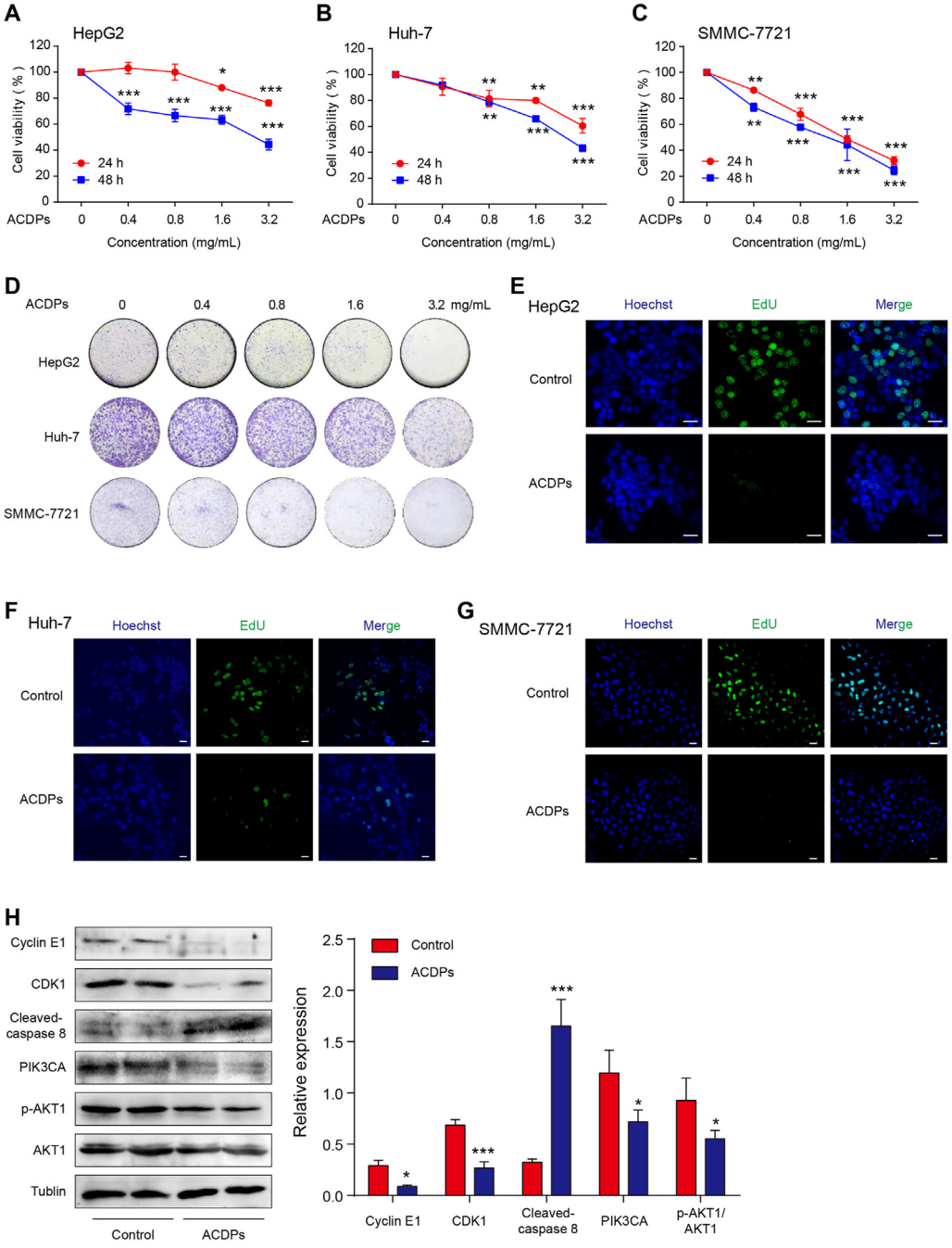

Figure 7 ACDPs repress the proliferation of HCC cells *in vitro* through PI3K/AKT/cell cycle axis. (A)–(C) CCK-8 for the viability of HCC cells, cultured in medium containing 0, 0.4, 0.8, 1.6, 3.2 mg/mL ACDPs for 24 and 48 h. Data are presented as mean ± SD, $*P < 0.05$, $**P < 0.01$ and $***P < 0.001$ compared to control group. (D) Colony formation experiments for the effect of ACDPs on the proliferation of HCC cells ($n = 6$). (E)–(G) EdU assay for the proliferation of HCC cells treated with the 3.2 mg/mL ACDPs or DMSO (control) for 24 h. Bar = 25 μm. (H) Western blot and densitometric analysis of expression of cyclin E1, CDK1, cleaved-caspase 8, PIK3CA, p-AKT1 and AKT1 in Huh-7 cells, cultured in medium containing 3.2 mg/mL ACDPs or DMSO for 24 h $*P < 0.05$, $***P < 0.001$ compared to control group.

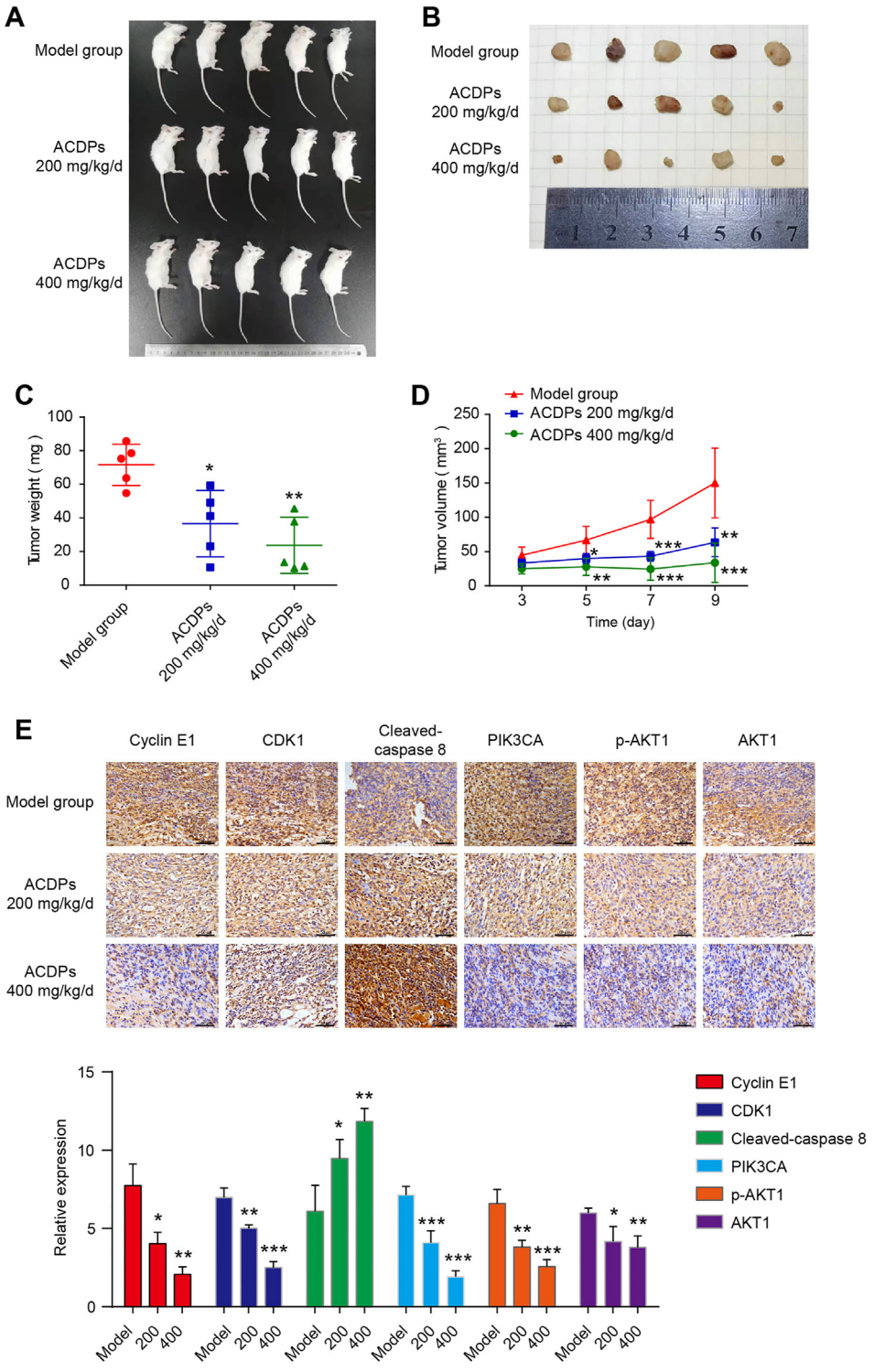

Figure 8 ACDPs inhibited tumor growth and downregulated the expression of cell cycle-related protein in HCC-xenograft mice. (A) and (B) The images of mice in each group and their corresponding transplanted tumors. (C) The effect of ACDPs on tumor weight of HCC-allograft mice ($n = 5$). *$P < 0.05$, **$P < 0.01$ compared to model group. (D) The effect of ACDPs on tumor volume of HCC-allograft mice ($n = 5$). *$P < 0.05$, **$P < 0.01$ and ***$P < 0.001$ compared to model group. (E) Immunohistochemistry analysis for the expression of cyclin E1, CDK1, cleaved-caspase 8, PIK3CA, p-AKT1 and AKT1 in tumor tissues from model and ACDPs group of HCC-allograft mice ($n = 5$). *$P < 0.05$, **$P < 0.01$ and ***$P < 0.001$ compared to model group. Bar = 50 μm.

anti-proliferation effect of ACDPs was confirmed by EdU assay (Fig. 7E−G). According to the results from the informatics, ACDPs might affect the expression of cell cycle-related proteins by regulating PI3K/AKT pathway. The expression of cyclin E1 and CDK1 in Huh-7 cell was detected by Western blot. As shown in Fig. 7H, they were significantly reduced after ACDPs-stimulation. We also found that the expression of cleaved-caspase eight was increased upon ACDPs-stimulation. Meanwhile, ACDPs decreased the expression of PIK3CA and the activity of AKT. In conclusion, ACDPs could exert an anti-cancer effect *via* PI3K/AKT signaling pathway in liver cancer.

3.6. ACDPs inhibited tumor growth and downregulated the expression of cell cycle-related protein in HCC-xenograft mice

To furtherly verify the antitumor effect of ACDPs and explore its possible mechanism *in vivo*, the HCC model of BALB/c mice was established. As shown in Fig. 8A and B, compared with the model group, ACDPs inhibits tumor growth in mice in a dose-dependent manner. Administration with 200 and 400 mg/kg/day ACDPs reduced tumor weight by 48% and 67% respectively, and significantly reduced tumor volume (Fig. 8C and D). The weight change curve of mice in each group was showed in Supporting Information Fig. S5, indicating that ACDPs had no obvious toxicity or side effects. Immunohistochemical staining was used to detect the expression levels of cell cycle-related proteins and the activity of PI3K/AKT signaling pathway. The expression levels of cyclin E1, CDK1, PIK3CA, p-AKT and AKT were significantly decreased, and that of cleaved-caspase eight was increased (Fig. 8E). Altogether, these data indicated that the ACDPs-induced the inhibition of cell proliferation was correlated with the induction of cell cycle arrest and the blockade of PI3K/AKT signaling pathway.

4. Discussion

HCC is one of the leading causes of cancer-related deaths worldwide, with more than 500,000 new cases annually, and its prevention and treatment still remains as a major clinical challenge. TCM has the characteristics of multiple targets and functions, and it has been widely used in the treatment of cancers because of its advantages, such as preferentially killing cancer cells, less side effect, less drug resistance, and improving the body's immunity. Extracts of *A. cinnamomea* has been reported to have anti-HCC activity *via* regulating cell apoptosis, viability, migration or invasion in a variety of liver cancers[11−14]. However, the main role of *A. cinnamomea* in anti-HCC and the relationship between the chemical components and targets remained remains to be not fully studied. In this study, we were the first to systematically analyze the chemical fingerprint in ACDPs. Drop pills are prepared by mixing medicinal plant extract with molten pharmaceutical base followed by dripping the mixture into an immiscible coolant until solidified droplets are achieved. The polymeric substance was detected in the MS chromatogram and shown as a zigzag peak, which are used to stabilize and increase bioavailability of the drug. The main peak in the chromatogram was polymeric substance as shown in Fig. S1. However, the presence of polymeric substance does not affect the identification of active ingredients in ACDPs. Using UPLC–Q-TOF/MS, 139 chemical components in ACDPs, including 102 terpenoids, eight benzenoids, two purine nucleosides and 27 other classes, were preliminarily determined. Next, it needs to be combined with the reference substance and other structural identification methods for accurate structural identification. Among of them, antcin A, antcin B, antcin C, antcin D, antcin K, antcin G, camphoratin C, camphoratin G, zhankuic acid B, zhankuic acid C, and Zhankuic acid E are the main ingredients. The whole process was rapid, efficient and accurate, suggesting the developed method could serve as a good strategy for qualitative analysis of the TCM with the advantage of high efficiency and sensibility.

On the basis of the chemical composition, composition-target network was established. The enrichment analysis of GO and KEGG were performed to analyze the targets of the active components of ACDPs. We found that these active components were enriched in cancer or cancer-related signal pathways, such as prostate cancer, pancreatic cancer, non-small cell lung cancer, cellular response to hypoxia, cellular response to hypoxia, TNF signaling pathway, inflammatory response, negative regulation of apoptotic process and positive regulation of cell proliferation, and so on. Next, though information biology analysis, 79 biomarkers of HCC were obtained from the database of GEO, TCGA and DisGeNET. AURKA, CCNB1, CDK1, SAE1 and TOP2A were the DEGs that significantly influenced the overall survival, and liver cancer patients with higher expression of these genes showed a worse prognosis. AURKA is an important regulator in mitotic progression, and frequently upregulated in HCC and other human cancers[33−35]. As is known to all, CCNB1 and CDK1 are absolutely essential for cell division and tumorigenesis. CCNB1 is a crucial G2/M phase promotor, and the cyclin B/CDK1 complex is the principal CDK that facilitates G2/M cell cycle transition[36]. SAE1 is a component of a heterodimeric small ubiquitin-related modifier that plays a vital role in SUMOylation, a post-translational modification involving in cellular events such as regulation of transcription, cell cycle and apoptosis. A recent study showed that SAE1 was overexpressed in HCC, and its overexpression was stage and grade-dependent and associated with poor survival[37]. TOP2A is one of the tumor drivers in a myriad of malignant tumors, and it increased cancer cell proliferation through inhibiting P53 activity[38]. TOP2A overexpression in HCC correlated with chemoresistance and shorter patients survival[39]. Finally, it is worth mentioning that, the most critical nine targets of ACDPs, CCNB1, CASP8, CCNE1, CDK1, PIK3CA, MET, AURKA, TOP2A and TERT, obtained by the final screening, and they were significantly enriched in PI3K/AKT and cell cycle signaling pathway, which might suggest the predominant role of ACDPs in suppressing HCC tumor progression.

Next, molecular docking is a theoretical simulation method that simulate the interaction of ligand and receptor, and predict the binding patterns and affinity. To investigate the interaction between ACDP bioactive compounds and target proteins, a molecular docking assay was carried out. The zhankuic acid E and ganoderiol B had the potentially high binding affinity with CDK1, PIK3CA, and zhankuic acid E and ganodermanontriol had the potentially high binding affinity with CCNE1, lucidumol A had the potentially high binding affinity with TERT, and so on. Zhankuic acid E, ganodermanontriol and lucidumol A belong to

triterpenoids, well known anti-tumor components[40,41]. At present, there are few studies about the relationship between zhankuic acid E and tumor. It is reported that other popular triterpenoids from *A.cinnamomea* plays key roles in anti-tumor, such as zhankuic acid A significantly improved the levles of G2/M arrest and sub G1 accumulation levels, trigging cell apoptosis and death of the resistant cell lines[42], zhankuic acid A and zhankuic acid C induced cell apoptosis in colon cancer cell lines HT-29 and SW-480[43,44]. The ganodermanontriol significantly promoted apoptosis of Hela and HepG2 cells[45,46], specifically suppressed proliferation in human breast cancer cells and colon cancer cells, and might be a potential chemotherapeutic agent for the treatment of cancer[47,48]. The lucidumol A reduced cell growth in Caco-2, HepG2 and HeLa cells in a dose-dependent manner[45]. Overall, the results from bioinformatics were accurate and feasible.

Finally, to verify these bioinformatics analysis results, a series of experiments were carried out. Herein, firstly, we found that ACDPs dose- and time-dependently inhibited the proliferation in multiple hepatocellular carcinoma cells, and exerted potent treatment effects on tumor growth in Huh7-cell-bearing mice, consisted with our previous prediction and the existing literatures about *A. cinnamomea*[10]. Then, according to bioinformatics that the anti-tumor efficacy of ACDPs might be related to its regulation on the PI3K/AKT/cell cycle axis, the results from Western blot of Huh-7 cells and immunohistochemistry of tumor tissues showed that ACDPs inhibited the expression of cell cycle-related protein and PIK3CA, decreased the activity of p-AKT, and upregulated the level of cleaved-caspase 8. Although a large number of studies have been reported the importance of PI3K/AKT pathway in liver cancer, very few have focused on the effect of *A. cinnamomea* on HCC PI3K/AKT pathway so far. It had been reported that ethanol extracts of fruiting bodies of *A. cinnamomea* suppressed the expressions of PI3K and phosphorylation of AKT in human adenocarcinoma cells[49,50], which was consistent with our study in HCC. It is known that the activation of PI3K/AKT signaling results in HCC cell proliferation, adhesion, migration, and invasion[51−54]. PI3K is activated through ligand binding, which phosphorylates AKT. PI3K/AKT signal pathway increased cyclin D1 and CDK4 expression, thereby promoting cell proliferation and cell-cycle G1/S transition[55,56]. In addition, PI3K/AKT directly triggers CDK1 activation, and promotes the entry of G2/M phase from S phase. Meanwhile, PI3K/AKT pathway was related to MDM2-P53 axis. MDM2 is one of the downstream proteins of AKT, and is phosphorylated by AKT, which causes the nuclear localization of MDM2 followed by its interaction with the tumor suppressor P53 and eventual degradation[57]. Therefore, ACDPs might downregulate cell cycle-related protein expression by inhibiting the PI3K/AKT signaling pathway, and PI3K/AKT/cell cycle axis may be the major pharmacological targets for ACDPs effects on anti-HCC.

5. Conclusions

In summary, a total of 139 chemical components are identified in ACDPs. Results from network pharmacology show that CCNB1, CASP8, CCNE1, CDK1, PIK3CA, MET, AURKA, TOP2A and TERT may be the potential protein targets, and molecular docking predicts the affinity between these targets and their corresponding active ingredients. KEGG pathway enrichment analysis reveal that the targets are significantly enriched in PI3K/AKT and cell cycle signaling pathway, which are verified by *in vivo* and *in vitro* experiments, suggesting that PI3K/AKT-mediated cell cycle progression plays the central role in the suppression of liver cancer of *A. cinnamomea*.

Acknowledgments

This work was supported by the National Key Research Project of China (2019YFC1606400), CAMS Innovation Fund for Medical Sciences (2019-I2M-5-055, China), Major Public Welfare Projects in Henan Province (201300110200, China), National Key Research Project of Hebei Province (20375502D, China), Natural Science Foundation of Hebei Province (H2019206212, China), High-level Talent Funding Project of Hebei Province (A201905006, China), Fund of National R & D Center for Edible Fungus Processing Technology, Henan University (20200109, China).

Author contributions

Bin Cong conducted experiments. Yan Zhang, Junmei Ma Xuqiang Liu and Sufang Fan identified the compounds of *A. cinnamomea*. Pin Lv, Ning Chen and Rong Wang planned and did *in vivo* and *in vitro* experiments, including treatment of tumor-bearing mice, cell culture, Western blot, cell viability assay, colony formation experiment and EdU assay. Huishan Guo and Xiaoruo Gan did Network pharmacological analysis. Yan Chen and Wenyi Kang did molecular docking. Yan Zhang, Wenyi Kang, Pin Lv and Junmei Ma analyzed data and wrote the manuscript. All authors read and approved the manuscript.

Conflicts of interest

The authors declare no potential conflicts of interest.

Appendix A. Supporting information

Supporting information to this article can be found online at https://doi.org/10.1016/j.apsb.2021.07.010.

References

1. Losic B, Craig AJ, Villacorta-Martin C, Martins-Filho SN, Akers N, Chen X, et al. Intratumoral heterogeneity and clonal evolution in liver cancer. *Nat Commun* 2020;**11**:291.
2. Zhang H, Dong P, Guo S, Tao C, Chen W, Zhao W, et al. Hypomethylation in HBV integration regions aids non-invasive surveillance to hepatocellular carcinoma by low-pass genome-wide bisulfite sequencing. *BMC Med* 2020;**18**:200.
3. Xiang Y, Guo Z, Zhu P, Chen J, Huang Y. Traditional Chinese medicine as a cancer treatment: modern perspectives of ancient but advanced science. *Cancer Med* 2019;**8**:1958−75.
4. Chung CH, Yeh SC, Tseng HC, Siu ML, Lee KT. Chemical quality evaluation of *Antrodia cinnamomea* fruiting bodies using phytomics similarity index analysis. *J Food Drug Anal* 2016;**24**:173−8.
5. Chen CC, Liu YW, Ker YB, Wu YY, Lai EY, Chyau CC, et al. Chemical characterization and anti-inflammatory effect of polysaccharides fractionated from submerge-cultured *Antrodia camphorata* mycelia. *J Agric Food Chem* 2007;**55**:5007−12.
6. Liu Y, Di X, Liu X, Shen W, Leung KS. Development of a LC–MS/MS method for the determination of antrodin B and antrodin C

from *Antrodia camphorata* extract in rat plasma for pharmacokinetic study. *J Pharmaceut Biomed Anal* 2010;**53**:781−4.
7. Chang CJ, Lu CC, Lin CS, Martel J, Ko YF, Ojcius DM, et al. *Antrodia cinnamomea* reduces obesity and modulates the gut microbiota in high-fat diet-fed mice. *Int J Obes (Lond)* 2018;**42**:231−43.
8. Chou WL, Lee TH, Huang TH, Wang PW, Chen YP, Chen CC, et al. Coenzyme Q(0) from *Antrodia cinnamomea* exhibits drug-resistant bacteria eradication and keratinocyte inflammation mitigation to ameliorate infected atopic dermatitis in mouse. *Front Pharmacol* 2019;**10**:1445.
9. Zhang Y, Ma AJ, Xi H, Chen N, Wang R, Yang C, et al. *Antrodia cinnamomea* ameliorates neointimal formation by inhibiting inflammatory cell infiltration through downregulation of adhesion molecule expression *in vitro* and *in vivo*. *Food Sci Hum Well* 2021;**10**:421−30.
10. Wu WD, Chen PS, Omar HA, Arafa ES, Pan HW, Jeng J, et al. *Antrodia cinnamome*a boosts the anti-tumor activity of sorafenib in xenograft models of human hepatocellular carcinoma. *Sci Rep* 2018;**8**:12914.
11. Zhu PL, Fu XQ, Li JK, Tse AK, Guo H, Yin CL, et al. *Antrodia camphorata* mycelia exert anti-liver cancer effects and inhibit STAT3 signaling *in vitro* and *in vivo*. *Front Pharmacol* 2018;**9**:1449.
12. Chen YY, Liu FC, Wu TS, Sheu MJ. *Antrodia cinnamomea* inhibits migration in human hepatocellular carcinoma cells: the role of ERp57 and PGK-1. *Am J Chin Med* 2015;**43**:1671−96.
13. Hsieh YC, Rao YK, Wu CC, Huang CF, Geethangili M, Hsu SL, et al. Methyl antcinate a from *Antrodia camphorata* induces apoptosis in human liver cancer cells through oxidant-mediated cofilin- and Bax-triggered mitochondrial pathway. *Chem Res Toxicol* 2010;**23**:1256−67.
14. Song TY, Hsu SL, Yen GC. Induction of apoptosis in human hepatoma cells by mycelia of *Antrodia camphorata* in submerged culture. *J Ethnopharmacol* 2005;**100**:158−67.
15. Huang GJ, Deng JS, Huang SS, Lee CY, Hou WC, Wang SY, et al. Hepatoprotective effects of eburicoic acid and dehydroeburicoic acid from *Antrodia camphorata* in a mouse model of acute hepatic injury. *Food Chem* 2013;**141**:3020−7.
16. Lee TH, Lee CK, Tsou WL, Liu SY, Kuo MT, Wen WC. A new cytotoxic agent from solid-state fermented mycelium of *Antrodia camphorata*. *Planta Med* 2007;**73**:1412−5.
17. Chang TT, Chou WN. *Antrodia cinnamomea* reconsidered and *A. salmomea*. *Bot Bull Acad Sin* 2004;**45**:347−52.
18. Huang HC, Liaw CC, Yang HL, Hseu YC, Kuo HT, Tsai YC, et al. Lanostane triterpenoids and sterols from *Antrodia camphorata*. *Phytochemistry* 2012;**84**:177−83.
19. Chiu HH. Phylogenetic analysis of *Antrodia* species and *Antrodia camphorata* inferred from internal transcribed spacer region. *Antonie Van Leeuwenhoek* 2007;**91**:267−76.
20. Cheng JJ, Yang CJ, Cheng CH, Wang YT, Huang NK, Lu MK. Characterization and functional study of *Antrodia camphorata* lipopolysaccharide. *J Agric Food Chem* 2005;**53**:469−74.
21. Nakamura N, Hirakawa A, Gao JJ, Kakuda H, Shiro M, Komatsu Y, et al. Five new maleic and succinic acid derivatives from the mycelium of *Antrodia camphorata* and their cytotoxic effects on LLC tumor cell line. *J Nat Prod* 2004;**67**:46−8.
22. Chen JJ, Lin WJ, Liao CH, Shieh PC. Anti-inflammatory benzenoids from *Antrodia camphorata*. *J Nat Prod* 2007;**70**:989−92.
23. Lu MK, Cheng JJ, Lai WL, Lin YR, Huang NK. Adenosine as an active component of *Antrodia cinnamomea* that prevents rat PC12 cells from serum deprivation-induced apoptosis through the activation of adenosine A(2A) receptors. *Life Sci* 2006;**79**:252−8.
24. Huang HS, Hsu JL, Yu CC, Chang LC, Chang CI. Qualitative and quantitative analysis of seven signature components in the fruiting body of *Antrodia cinnamomea* by HPLC−ESI-MS/MS. *Acta Chromatogr* 2016;**28**:387−402.
25. Daina A, Michielin O, Zoete V. SwissADME: a free web tool to evaluate pharmacokinetics, drug-likeness and medicinal chemistry friendliness of small molecules. *Sci Rep* 2017;**7**:42717.
26. Gfeller D, Grosdidier A, Wirth M, Daina A, Michielin O, Zoete V. SwissTargetPrediction: a web server for target prediction of bioactive small molecules. *Nucleic Acids Res* 2014;**42**:W32−8.
27. Luan X, Wang Y. LncRNA XLOC_006390 facilitates cervical cancer tumorigenesis and metastasis as a ceRNA against miR-331-3p and miR-338-3p. *J Gynecol Oncol* 2018;**29**:e95.
28. Chen X, Yang J, Wang Y. LncRNA JPX promotes cervical cancer progression by modulating miR-25-3p/SOX4 axis. *Cancer Cell Int* 2020;**20**:441.
29. Chien SC, Chen ML, Kuo HT, Tsai YC, Lin BF, Kuo YH. Anti-inflammatory activities of new succinic and maleic derivatives from the fruiting body of *Antrodia camphorata*. *J Agric Food Chem* 2008;**56**:7017−22.
30. Chen CC, Shiao YJ, Lin RD, Shao YY, Lai MN, Lin CC. Neuroprotective diterpenes from the fruiting body of *Antrodia camphorata*. *J Nat Prod* 2006;**69**:689−91.
31. Geethangili M, Tzeng YM. Review of pharmacological effects of *Antrodia camphorata* and its bioactive compounds. *Evid Based Complement Alternat Med* 2011;**2011**:212641.
32. Liu XX, Hua Z, Zhang ZF, Wang XF. LC–MS determination of organic acids in fruits and vegetables. *The Food Industry* 2016;**5**:289−93.
33. Giet R, Prigent C. Aurora/Ipl1p-related kinases, a new oncogenic family of mitotic serine-threonine kinases. *J Cell Sci* 1999;**112 Pt 21**:3591−601.
34. Carmena M, Earnshaw WC. The cellular geography of aurora kinases. *Nat Rev Mol Cell Biol* 2003;**4**:842−54.
35. Seki A, Coppinger JA, Jang CY, Yates JR, Fang G. Bora and the kinase Aurora a cooperatively activate the kinase Plk1 and control mitotic entry. *Science* 2008;**320**:1655−8.
36. Carmichael J, DeGraff WG, Gazdar AF, Minna JD, Mitchell JB. Evaluation of a tetrazolium-based semiautomated colorimetric assay: assessment of chemosensitivity testing. *Cancer Res* 1987;**47**:936−42.
37. Ong JR, Bamodu OA, Khang NV, Lin YK, Yeh CT, Lee WH, et al. SUMO-activating enzyme subunit 1 (SAE1) is a promising diagnostic cancer metabolism biomarker of hepatocellular carcinoma. *Cells* 2021;**10**:178.
38. Liu T, Zhang H, Yi S, Gu L, Zhou M. Mutual regulation of MDM4 and TOP2A in cancer cell proliferation. *Mol Oncol* 2019;**13**:1047−58.
39. Wong N, Yeo W, Wong WL, Wong NL, Chan KY, Mo FK, et al. TOP2A overexpression in hepatocellular carcinoma correlates with early age onset, shorter patients survival and chemoresistance. *Int J Cancer* 2009;**124**:644−52.
40. Tran TA, McCoy MK, Sporn MB, Tansey MG. The synthetic triterpenoid CDDO-methyl ester modulates microglial activities, inhibits TNF production, and provides dopaminergic neuroprotection. *J Neuroinflammation* 2008;**5**:14.
41. Jannus F, Medina-O'Donnell M, Rivas F, Díaz-Ruiz L, Rufino-Palomares EE, Lupiáñez JA. A diamine-PEGylated oleanolic acid derivative induced efficient apoptosis through a death receptor and mitochondrial apoptotic pathway in HepG2 human hepatoma cells. *Biomolecules* 2020;**10**:1375.
42. Teng YN, Wang YH, Wu TS, Hung HY, Hung CC. Zhankuic acids A, B and C from taiwanofungus camphoratus act as cytotoxicity enhancers by regulating p-glycoprotein in multi-drug resistant cancer cells. *Biomolecules* 2019;**9**:759.
43. Yeh CT, Rao YK, Yao CJ, Yeh CF, Li CH, Chuang SE. Cytotoxic triterpenes from Antrodia camphorata and their mode of action in HT-29 human colon cancer cells. *Cancer Lett* 2009;**285**:73−9.
44. Liu DZ. A review of ergostane and cucurbitane triterpenoids of mushroom origin. *Nat Prod Res* 2014;**28**:1099−105.
45. Ruan W, Wei Y, Popovich DG. Distinct responses of cytotoxic *Ganoderma lucidum* triterpenoids in human carcinoma cells. *Phytother Res* 2015;**29**:1744−52.
46. Xu C, Guo H, Kong D, Pang D, Ding Y. Ganodermanontriol inhibits expression of special AT rich sequence binding protein 1 gene in human hepatocellular carcinoma. *J Cancer Res Ther* 2018;**14**:S964−8.

47. Jiang J, Jedinak A, Sliva D. Ganodermanontriol (GDNT) exerts its effect on growth and invasiveness of breast cancer cells through the down-regulation of CDC20 and uPA. *Biochem Biophys Res Commun* 2011;**415**:325−9.
48. Jedinak A, Thyagarajan-Sahu A, Jiang J, Sliva D. Ganodermanontriol, a lanostanoid triterpene from *Ganoderma lucidum*, suppresses growth of colon cancer cells through *β*-catenin signaling. *Int J Oncol* 2011;**38**: 761−7.
49. Chen YY, Chou PY, Chien YC, Wu CH, Wu TS, Sheu MJ. Ethanol extracts of fruiting bodies of *Antrodia cinnamomea* exhibit anti-migration action in human adenocarcinoma CL1-0 cells through the MAPK and PI3K/AKT signaling pathways. *Phytomedicine* 2012;**19**: 768−78.
50. Chen YY, Liu FC, Chou PY, Chien YC, Chang WW, Huang GJ, et al. Ethanol extracts of fruiting bodies of *Antrodia cinnamomea* suppress CL1-5 human lung adenocarcinoma cells migration by inhibiting matrix metalloproteinase-2/9 through ERK, JNK, p38, and PI3K/Akt signaling pathways. *Evid Based Complement Alternat Med* 2012; **2012**:378415.
51. Chang AY, Wang M. Molecular mechanisms of action and potential biomarkers of growth inhibition of dasatinib (BMS-354825) on hepatocellular carcinoma cells. *BMC Cancer* 2013;**13**:267.
52. Hindupur SK, Colombi M, Fuhs SR, Matter MS, Guri Y, Adam K. The protein histidine phosphatase LHPP is a tumour suppressor. *Nature* 2018;**555**:678−82.
53. Engelman JA, Luo J, Cantley LC. The evolution of phosphatidylinositol 3-kinases as regulators of growth and metabolism. *Nat Rev Genet* 2006;**7**:606−19.
54. Lien EC, Dibble CC, Toker A. PI3K signaling in cancer: beyond AKT. *Curr Opin Cell Biol* 2017;**45**:62−71.
55. Gao N, Flynn DC, Zhang Z, Zhong XS, Walker V, Liu KJ, et al. G1 cell cycle progression and the expression of G1 cyclins are regulated by PI3K/AKT/mTOR/p70S6K1 signaling in human ovarian cancer cells. *Am J Physiol Cell Physiol* 2004;**287**: C281−91.
56. Wang H, Wu Q, Liu Z, Luo X, Fan Y, Liu Y, et al. Downregulation of FAP suppresses cell proliferation and metastasis through PTEN/PI3-K/AKT and Ras-ERK signaling in oral squamous cell carcinoma. *Cell Death Dis* 2014;**5**:e1155.
57. Singh S, Ramamoorthy M, Vaughan C, Yeudall WA, Deb S, Deb SP. Human oncoprotein MDM2 activates the Akt signaling pathway through an interaction with the repressor element-1 silencing transcription factor conferring a survival advantage to cancer cells. *Cell Death Differ* 2013; **20**:558−66.